Experimental and theoretical studies of the physicochemical and mechanical properties of multi-layered TiN/SiC films: Temperature effects on the nanocomposite structure

Article *in* Composites Part B Engineering · June 2018

DOI: 10.1016/j.compositesb.2018.01.004

CITATIONS
6

READS
275

8 authors, including:

Alexander Pogrebnjak
Sumy State University
287 PUBLICATIONS **2,691** CITATIONS
SEE PROFILE

Volodymyr Ivashchenko
National Academy of Sciences of Ukraine
107 PUBLICATIONS **685** CITATIONS
SEE PROFILE

Petro Scrynskyy
National Academy of Sciences of Ukraine
22 PUBLICATIONS **61** CITATIONS
SEE PROFILE

Oleksandr V. Bondar
Sumy State University
59 PUBLICATIONS **387** CITATIONS
SEE PROFILE

Composites Part B 142 (2018) 85–94

Contents lists available at ScienceDirect

Composites Part B

journal homepage: www.elsevier.com/locate/compositesb

Experimental and theoretical studies of the physicochemical and mechanical properties of multi-layered TiN/SiC films: Temperature effects on the nanocomposite structure

Alexander D. Pogrebnjak[a,*], Volodymyr I. Ivashchenko[b], Petro L. Skrynskyy[b], Oleksandr V. Bondar[a], Piotr Konarski[c], Karol Załęski[d], Stefan Jurga[d,e], Emerson Coy[d,**]

[a] Sumy State University, R.-Korsakova 2, 40007 Sumy, Ukraine
[b] Frantsevych Institute for Problems of Material Science, NAS of Ukraine, 3, Krzhyshanovsky Str., 03142 Kyiv, Ukraine
[c] Tele and Radio Research Institute, ul. Ratuszowa 11, 03-450 Warsaw, Poland
[d] NanoBioMedical Centre, Adam Mickiewicz University, ul. Umultowska 85, 61614 Poznań, Poland
[e] Department of Macromolecular Physics, Adam Mickiewicz University, ul. Umultowska 85, 61614 Poznań, Poland

ARTICLE INFO

Keywords:
Nitrides
Carbides
Heterostructures
Thin films
Molecular dynamics simulations
Composite materials

ABSTRACT

Nanoscale multilayered TiN/SiC films are of great importance in many electronic and industrial fields. The careful control over the structure of the laminates, nanocrystalline or amorphous, is crucial for their further applicability and study. However, several limitations in their fabrication have revealed important gaps in the understanding of this system. Here, we study influence of temperature on the physico-chemical and functional properties of TiN/SiC multilayers. We will show the clear increment on hardness of the samples, while the nanocomposite structure of the layers is maintained with no increment in crystal size. We will investigate the interstitial effects and rearrangements, between the TiN/SiC phases and their role in the enhanced mechanical response. Our experiments will clearly show a change in the modulation period of the samples, pointing to interfacial reactions, diffusion of ions or crystallization of new phases. Full Investigations of the film properties were carried out using several methods of analysis: XRD, XPS, FTIR, HR-TEM and SIMS Additionally, results were combined with First Principles MD computations of TiN/SiC heterostructures.

1. Introduction

Nitrides occupy a privilege place in the both the industry and the academy, because of their unique and versatile properties [1–4]. Nevertheless, in fields that demand high mechanical, thermal and electrical resilience, the physical, mechanical, and tribological properties of conventional ceramic hard and wear-resistant protective coatings, such as titanium nitride (TiN), are not sufficient to prevent catastrophic failure in extreme mechanical-loading conditions due to material brittleness (I.e. crack formation and propagation upon loading single-crystal B1-TiN(001) ($Fm\bar{3}m$-225) and VN(001) layers [5]). A common strategy to address the problem of inherent brittleness in ceramics, consists in enhancing hardness/toughness by alloy or multilayer design [6–9] or via control of the electronic structure [10–13]. This, however, does not guarantee that the protective properties are maintained at high temperatures, since the hardness and stiffness of a single-phase compound or solid solution typically decrease monotonically with increasing temperature [14]. Hot hardness needs to be combined with improved toughness, which is generally achieved by controlling solid solution thermal stability, however, this leads to spinodal decomposition at high temperatures [15–19]. Nevertheless, the hardness achieved in the works listed above typically does not exceed ~35 GPa. The necessity of improving material protective performances continuously motivates research toward development of new superhard ($H > 40$ GPa) materials with enhanced wear and corrosion resistance combined with resistance to thermally-induced stresses [20–23]. On the other hand, nanocomposite coatings have shown improved toughness and fracture resistance, that although have provided a broad range of applications to materials, remain below the superhard values [24–30]. Nevertheless, H.W. Hugosson et al. [31] have theoretically shown that by promoting stacking-fault or multiphase interfaces, the hardness of the protective coatings can be enhanced, mainly due to the stabilization of interfacial phases and the major role that coherent interfaces can play in the stabilization of low-energy interfaces and nanodomains

* Corresponding author.
** Corresponding author.
E-mail addresses: alexp@i.ua (A.D. Pogrebnjak), coyeme@amu.edu.pl (E. Coy).

https://doi.org/10.1016/j.compositesb.2018.01.004
Received 29 November 2017; Received in revised form 16 January 2018; Accepted 16 January 2018

[32], these facts show the relevance of interfacial/granular electronic structure in high performance protective coatings [33,34].

Silicon carbide (SiC) and different composite materials based on it are currently among the most promising materials for industrial applications [35–37]. Due to their unique combination of physico-chemical properties, such as chemical stability, refractoriness, wear and radiation resistance, SiC-based protective coatings are widely demanded in machine-building, nuclear energy, metallurgical, chemical, gas, petroleum and petrochemical industries. Intensive studies devoted to the development of composite materials based on non-oxide compounds, such as carbon, silicon carbide or nitride, in combination with carbides or nitrides of refractory metals, are carried out actively at present [38,39]. Such compounds can be used as matrices or as reinforcing filler in the form of fibres or plates [40,41]. These composite materials are characterized by low specific mass, durability and wear resistance, and demonstrate the possibility of forming complex shapes with sharp details. Due to their high strength and heat resistance, they can be used in the aeronautics and space industries as high-temperature construction materials for gas turbines, petrol engines, heat exchangers production, *etc*. SiC is widely used in modern electronics as semiconducting material in superfast high-voltage Schottky diodes, MOSFET transistors and high-temperature transistors. Higher electric strength, larger band gap, higher permissible operating temperature, thermal conductivity and resistance to irradiation are among the main advantages of SiC in comparison with traditional materials, such as Silicon, Gallium arsenide, *etc* [42]. It is also worth mentioning that the combination of excellent electronic and mechanical properties offers many opportunities to use SiC as a material for a wide range of devices and sensors subjected to high temperatures or corrosive media, for example, regulators of electricity distribution, combustion process controllers, and uncooled radiation detectors for the new generation of aerospace materials.

Superhard heterostructures based on transition metal compounds have been thoroughly investigated during the last decade due to their exceptional applicability in electronics [43–46] and protective coatings [47]. Among them, TiN/SiN_x, ZrN/SiN_x and TiN/AlN heterostructures (nanoscale multilayers) are among the most studied systems [48–55]. It has been shown that a thin interfacial layer of B1 (rocksalt structure) SiN_x and B1-AlN can be formed between TiN layers [54]. TiN/SiC heterostructures have been studied to a lesser extent. To our knowledge, only three previous investigations have been devoted to the experimental and theoretical studies of the structural and mechanical properties of TiN/SiC nanolayered systems [56–58]. The authors [56,57] deposited nanoscale multilayer TiN/SiC films by r.f. magnetron sputtering at room temperature. They showed that the epitaxial B1-SiC ($Fm\bar{3}m$-225) interfacial layers were formed between TiN slabs when the thickness of the SiC layers was less than 0.6–0.8 nm [56]. However, in subsequent investigations [57] the same authors revised the conclusions of their previous work [56], stating that the interfacial layer had the B3-SiC ($F\bar{4}3m$-216) Zinc blende structure. According to these reports [56,57] the crystallization of SiC (for the exact thickness of 0.6 nm, not less or greater) and the epitaxial growth between TiN and SiC layers are responsible for high hardness, which reached the value of 60 GPa. At the same time, in Ref. [57] authors presented the dependencies of hardness HV (GPa) on thickness of the TiN layers, which changed from 2.5 to 19.8 nm, while thickness of SiC remained fixed to 0.6 nm. Hardness of the coatings remained around 40 GPa for various thicknesses of the TiN layers (from 9.5 to 19.8 nm), while nanohardness reaches the values around 18 GPa. The dependencies of the universal hardness (HU) on the indenter penetration depth are provided, when the thickness of SiC changes from 0.4 to 2.4 nm, while the thickness of TiN layers remains fixed [56,57]. The theoretical study of the TiN (001)/monolayer B1-SiC heterostructure showed that it was thermally stable up to 600 K [58], whereas the interface in the TiN(111)/monolayer B1-SiC heterostructure transformed to the B3-SiC structure even at low temperatures [58]. Nevertheless, possibility of recrystallizing thicker SiC layers has not yet been addressed. This issue remains as one of the most restrictive parameters for further implementation of SiC heterostructures in electronics and protective coatings [59–61].

Taking into account the remarkable experimental results achieved for the TiN/SiC nanolayered films deposited at room temperature [56,57], we deposited TiN/SiC nanoscale multilayers to establish the role of substrate temperature in the structural and mechanical properties of the films. In our study we have increased the thickness of SiC to ≈5 nm, in order to provide a fresh perspective on the crystallization dynamics of thicker layers. The aim of the present study is to investigate the influence of substrate temperature during deposition on the structure and properties of the fabricated TiN/SiC coatings via detailed experimental analyses based on XRD, XPS, FTIR, STEM, HRTEM and SIMS, which provide complementary information. Correspondingly, atomic-scale understanding of phenomena responsible for the improved properties is achieved via ab initio molecular dynamics (MD) simulations [62]. Here, we show that thicker layers of SiC are not amorphous, but show a nanocomposite structure, with small crystals embedded in amorphous phase, and that by a rather low temperature process, it is possible to improve the physico-chemical interactions between SiC and TiN layers, leading to an improved mechanical response of the samples, comparable to the response observed in super hard composites. Our results provide several novel insights for clarifying key mechanisms governing the formation and mechanical properties of modern multilayered nanoscale protective coatings.

2. Experimental and computational details

2.1. Preparation of the coatings

TiN/SiC nanoscale multilayered films were deposited by consecutive DC magnetron sputtering steps from TiN and SiC targets (72 mm diameter and 4 mm thick disks with purity of 99.9%) at different substrate temperatures, T_S = 25, 100, 200 and 350 °C (samples S-25, S-100, S-200 and S-350, respectively). In addition, single-layer TiN and SiC 700 nm films were deposited at T_S = 350 °C. The distance between the targets and the substrate holder was kept constant at 8 cm. The substrates were polished Si (100) wafers. Before the deposition, the silicon wafers were cleaned in a bath with a 5% HF solution to remove the native oxide. Afterwards, the substrates were rinsed in de-ionized water and dried in nitrogen. Finally, they were sputter-etched in argon plasma in the reaction chamber prior to deposition. The substrate bias was −50 V. The argon flow rate and working pressure were 60 sccm and 0.2 Pa, respectively. The DC power density (discharge power) values at the TiN and SiC targets were 1.72 W/cm^2 and 0.86 W/cm^2, respectively. In the case of the nanoscale multilayered films, the TiN and SiC layers were deposited for 2 min and 1 min, respectively. The total number of layers was 116. The working pressure was 10^{-3} Pa.

2.2. Experimental analyses and procedures

X-ray diffraction (XRD) investigations of the films were performed with a diffractometer “PANanalytical” using Cu K_α radiation. Low angle XRD (LAXRD) was used to analyse the layer structure of the multilayer films (Ultima IV “Rigaku”, Cu K_α radiation). X-ray reflectometry (XRR) measurements were performed on the X'pert^3 MRD (XL) from PANalytical with a Cu Kα radiation source (wavelength of 1.54 Å) operating at 45 kV and 40 mA. The chemical bonding was studied by Fourier transform infrared spectroscopy (FTIR) (with a “FSM 1202” LLC “Infraspek” spectrometer). The chemical states were studied by an EC 2401 X-ray photoelectron spectroscopy (XPS) system using Mg K_α X-ray radiation (E = 1253.6 eV). The Au $4f_{7/2}$ and Cu $2p_{3/2}$ peaks with binding energies of 84.0 ± 0.1 eV and 932.66 ± 0.05 eV, respectively, were used as a reference. The pass energy was 50 eV and resolution of 0.1 eV. The films were etched for 5 min with 1.8 keV Ar^+ ions to remove surface contaminations. The structural properties of the

films were investigated by transmission electron microscopy (TEM) (JEOL ARM 200 F high-resolution transmission electron microscope (200 kV) with an EDX analyser). The cross sections and lamellae for TEM investigations were prepared by a focused ion beam (FIB) method. The FIB milling was carried out with a JEOL JIB-4000. A broad carbon thin film was deposited on the sample surface to protect the area of interest from damage during the FIB milling and observation with the Ga^+ ion beam. The Ga^+ ion beam of adjustable acceleration voltage (5–30 kV) was used to prepare lamellae down to electron transparency. Secondary ion mass spectroscopy (SIMS) measurements were carried out on a SAJW-05 analyser [63] equipped with a Physical Electronics 06-350E ion gun and QMA-410 Balzers quadrupole mass analyser. We used an argon ion beam of 1.72 keV at a 45° incidence angle, digitally scanned over a 1 mm × 1 mm area. For depth profile analysis, we selected positive secondary ion currents emitted from the central part of the scanned area (15% electronic gate). The selected masses were 12, 14, 16 and 48 D. The masses of 12, 16 and 48 represent secondary ions, $^{12}C^+$, $^{16}O^+$ and $^{48}Ti^+$ respectively, while the mass of 14 represents $^{12}CH_2{}^+$ or $^{28}Si^{++}$ ions rather than $^{14}N^+$.

The nanoindentation of the films was carried out under continuous stiffness measurements (CSM) mode using a Nano Indenter-G200 system (Agilent Technologies) and Triboindenter TI-950 (Hysitron). This mode allows one to perform a continuous measurement of the contact stiffness via a superimposed alternating current signal during loading, which, in turn, provides a continuous measurement of the elastic modulus (E) and hardness (H) as functions of indenter displacement (L) during a single loading segment [64]. All nanoindentation measurements were performed using a Berkovich diamond tip with a nominal radius of ~340 nm. The area function was calibrated from indentation on a standard fused silica specimen. Eight indentations were made on each sample. The load and displacement were continuously recorded up to a maximum displacement of 200 nm at a constant indentation strain rate of 0.05 s^{-1}. The CSM frequency was 45 Hz, and the amplitude of oscillation was 2 nm. The nanohardness and elastic modulus were determined as the maximum values in the H (L) and E(L) dependences, respectively, in the range of $0 < L < 0.1$ D (where D is the thickness of the films). Knoop hardness (HK) was determined by a MICROMET 2103 Microhardness Tester device (BUEHLER, USA) at a load of 100 mN, and the hardness value for each specimen was an average of at least 10 measurements. The thickness of the films was estimated by a Micron-alpha optical profilometer (Ukraine). The film thicknesses were approximately 1.0 μm, and slightly decreased with increasing T_S. The scratch tests were performed with a Micron-gamma scratch tester (Ukraine) using a Vickers diamond pyramidal tip with a linear scan rate of 9 μm/s and a ramping load from 0 to 0.3 N.

2.3. Computational details

To investigate the structure of the TiN(001)/SiC interface, we considered the initial (2 × 2 × 3) 96-atom supercell constructed of the 8-atom B1(NaCl)-TiN cubic unit cells. The interfacial B1-SiC layers were introduced by replacing Ti and N atoms with Si and C atoms, respectively, in the three central lattice planes perpendicular to the c-axis. Thus, our heterostructures are formed of alternating 48-atom B1 SiC(001)/96-atom B1 TiN(001) layers.

The calculations were performed using the first-principles pseudopotential DFT MD method as implemented in the quantum ESPRESSO code [65] with periodic boundary conditions [54,66]. The generalized gradient approximation (GGA) of Perdew, Burke, and Ernzerhof [67] was used to evaluate the electronic exchange-correlation energy, and the Vanderbilt ultra-soft pseudo-potentials were used to describe the electron-ion interaction [68]. The non-linear core corrections were taken into account as described in the literature [65]. The criterion of convergence for the total energy was 10^{-6} Ry/formula unit ($1.36{\cdot}10^{-5}$ eV). To speed up the convergence, each eigenvalue was convolved with a Gaussian of a width of $\delta = 0.02$ Ry (0.272 eV). The cut-off energy for the plane-wave basis E_{cut} was 30 Ry (408 eV) and the Monkhorst-Pack [69] mesh of 2 × 2 × 2 k-points was used for Brillouin zone sampling.

All the structures were optimized by simultaneously relaxing the atomic basis vectors and the atomic positions inside the unit cells using the Broyden-Fletcher-Goldfarb-Shanno (BFGS) algorithm [70]. The relaxation of the atomic coordinates and of the unit cell is considered to be complete when the atomic forces are less than 1.0 mRy/Bohr (25.7 meV/Å), the stresses are smaller than 0.05 GPa, and the total energy during the structural optimization iterative process changed by less than 0.1 mRy (1.36 meV).

The initial relaxed TiN(001)/SiC heterostructure was: i) equilibrated at 300 K and then relaxed (denoted B1); ii) equilibrated at 1200 K, slowly cooled to 300 K and then relaxed (denoted B3). We carried out molecular dynamics (MD) simulations with a 48 atom B1-SiC sample to generate amorphous silicon carbide. To do this, the sample was heated up to 4500 K, equilibrated, cooled to 300 K and then relaxed (denoted a-SiC). This layer was inserted into the initial 96 atom TiN(001)/SiC heterostructure instead of the 48 atom B1-SiC layer. Two samples of the TiN(001)/a-SiC heterostructure were generated. The initial relaxed TiN(001)/a-SiC heterostructure was: i) equilibrated at 300 K and then relaxed (denoted A0); equilibrated at 1200 K, slowly cooled to 300 K and then relaxed (denoted A1). The quantum MD (QMD) equilibration of all the structures at each temperature was performed for 2 ps in the NPT ensemble (with the number of particles, pressure, and temperature all held constant). An exception was made for the a-SiC sample: this structure was generated in the NVT ensemble (with the number of particles, volume, and temperature all held constant). The system temperature is kept constant by rescaling the velocity. In all the MD calculations, the time step was 20 atomic units (a.u., approximately 10^{-15} s). The variation of the total energy during each QMD time step was controlled. During the initial 1.2–1.5 ps, all structures reached close to their equilibrium state and, at later times, the total energy and the supercell volume oscillate around the equilibrium values.

The pseudo-potential procedure was used to study the phonon dispersion curves for the two atom B1-SiC unit cell at various lattice parameters in the framework of the density-functional perturbation theory (DFPT) described in Refs. [65,71].

The tensile stress-strain relations were calculated by: 1) elongating the supercells along the c-axis [(001)-direction] in an incremental step, 2) fixing of the **c** basis cell vector and 3) simultaneously relaxing the **a**- and **b**-basis cell vectors and the positions of the atoms within the supercell. The structural parameters at a previous step were used to calculate the Hellmann-Feynman stress for the next step.

3. Results and discussion

3.1. Experimental results

We carried out the deposition of TiN and SiC monolayer films as well as TiN/SiC multilayer films under the same conditions. In Fig. 1, we show the FTIR spectra of SiC films deposited at 25 °C and 350 °C substrate temperatures. Given this finding, and taking into account the fact that the main areas of absorption are caused by vibrations at 770 cm^{-1} (Si-C vibrations) and at 1000 cm^{-1} (Si-O vibrations) [72], we aim at a conclusion that the bonding configuration of the SiC films represents the amorphous Si-C-O network. The absorption band at 1000 cm^{-1} decreases with increasing T_S. It follows that a moderate increase in substrate temperature promotes a reduction of the number of Si-O bonds.

Grazing Incident XRD diffractograms of the nanoscale multilayered films deposited at various substrate temperatures are shown in Fig. 2 in comparison with the XRD diffractogram of the single-layered TiN film. The XRD patterns of the low temperature multilayered films deposited

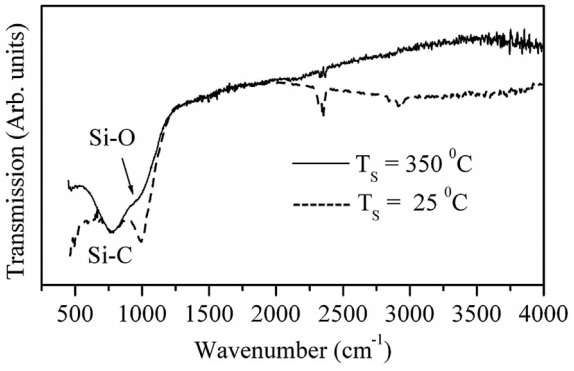

Fig. 1. FTIR spectra of SiC films deposited at different substrate temperatures (T_S).

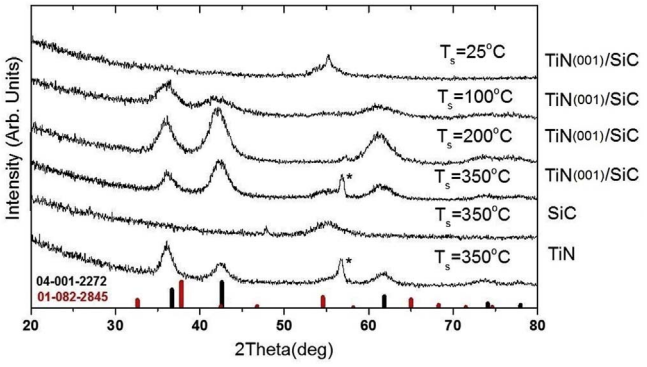

Fig. 2. GI-XRD difractograms of TiN/SiC nanolayered, SiC and TiN monolayer films deposited at different substrate temperatures (T_S). Red lines correspond to SiC and black to TiN, * shows a hexagonal phase. (For interpretation of the references to colour in this figure legend, the reader is referred to the Web version of this article.)

at T_S = 25 and 100 °C demonstrate a weak reflex at 2Θ = 36.5°, which can be attributed to small crystallites of TiN rapidly appearing with the temperature increment. There are no crystallites related to silicon carbide in these films. Thus, one can suppose that the low temperature films represent the sequence of the nanocrystalline TiN layers with tiny grains separated by amorphous silicon carbide layers. High-temperature nanolayered films, however, deposited at T_S = 200 and 350 °C, particularly XRD patterns of these films, indicate the formation of nanocrystalline TiN layers with larger grains than in the low-temperature films. In the XRD spectrum of the nanolayered film deposited at 350 °C, the small peaks at 2Θ = 35.6°, 40.5°, 41.5°and 65.8° are attributed to the reflexes related to the small crystallites of hexagonal and cubic (3C-SiC) silicon carbides [PDF files 073–2082, 029–1131, 074–2307, 082–2845]. The reflections at 2Θ = 36.4° and 42.3° in the high-angle XRD spectra of this film and the TiN film indicate the presence of the B1-TiN phase in these films [PDF file 001–2272]. Both films demonstrate slight (001) textures (cf. Fig. 2). These findings allow us to assume that the high temperature film should be regarded as nc-TiN/nc-SiC (nc-nanocrystalline) multilayers. This leads to the conclusion that the substrate temperature of 350 °C, under the experimental conditions of this work, is a threshold temperature at which the amorphous SiC layers begin to crystallize. It should be noted, however, that monolayer SiC films deposited at T_S = 350 °C are highly amorphous (cf. Fig. 1), whereas the SiC layers in the multilayers are nanocrystalline due to the presence of the crystalline structure of the TiN layers. Additionally, by using the Scherrer equation ($\tau = K\lambda/\beta cos\theta$), the overall grain size can be estimated. K is the shape factor, λ is Cu wavelength, β is the experimental FWHM and θ the Bragg angle. Grain size is estimated as 3.35 ± 0.5 nm, which suggest that temperature does not promote crystal growth but atom mobility or new nucleation.

The XRR patterns of the high temperature multilayered films, shown in Fig. 3, clearly indicate the existence of a compositional layered structure of multilayers. From the Θ/2Θ position of the superlattice peaks, the modulation periods Λ were determined by a modified form of Bragg's law: $Sin(\Theta_m) = m\lambda/2\Lambda$, where m is the order of the reflection, and λ is the X-ray wavelength [73]. The values of Λ for the films deposited at 200 °C and 350 °C were calculated to be between 17.42 nm and 16.58 nm, respectively, which means that the modulation period slightly decreases with increasing substrate temperature. This could be an effect from the increase in the portion of nanocrystalline phases in SiC layers in the high temperature film. As a result, the modulation period expands from 11.50 nm (m = 1) to 14.89 nm (m = 2) for the S-200 film, and from 11.41 nm (m = 1) to 14.53 nm (m = 2) for the S-350 film. For m > 3, the modulation period oscillates approximately 17.42 nm and 16.58 nm for the S-200 and S-350 films, respectively.

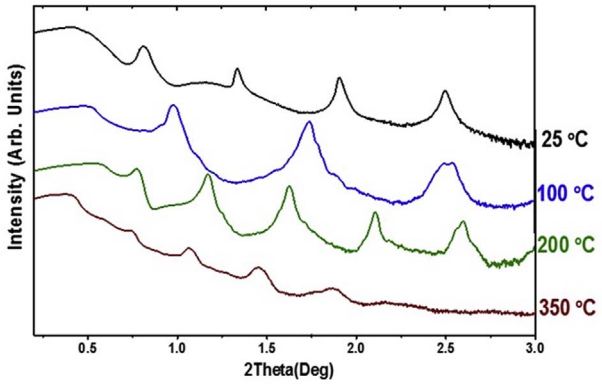

Fig. 3. X-ray reflectometry (XRR) patterns of compositional layered structure of TiN/SiC nanolayered films deposited at given substrate temperatures: 25 °C, 100 °C, 200 °C and 350 °C.

The cross-sectional transmission electron microscope (TEM) images and the selected area diffraction patterns (SAED) taken from the S-350 film are shown in Fig. 4. The film shows a composition modulated structure, comprising the light $TiN_{(12 \pm 0.5\ nm)}$ and dark $SiC_{(3 \pm 0.5nm)}$ layers, which contrast with the S-25 sample and its $TiN_{(7.3 \pm 0.5\ nm)}$ and $SiC_{(4.5 \pm 0.5\ nm)}$, clearly correlating with the modulation changes due to substrate temperature. The film has a total thickness of 0.96 μm with excellent periodicity. The self-correlation analysis (cf. inset in Fig. 4) shows that Λ is approximately equal to 16.7 nm, in good agreement with the modulation period of 16.58 nm obtained from the XRR difractograms.

In Fig. 5, we demonstrate the diffraction patterns collected over a 200 nm^2 area of the Si substrate for the S-350 film and the S-200 film. The diffraction lines of the film show polycrystallinity very small nanocrystals containing both SiC and TiN diffraction peaks. The silicon patterns are presented on the left side of Fig. 5 to investigate the possibility of any ordering or textured growth; however, the samples do not show such features. Nevertheless, the SAED patterns from the films show an inverse trend in nanocrystalline size with temperature; well defined spots are present in each ring of diffraction from the sample 200 °C, in contrast with the featureless 300 °C sample, supporting the XRD observations, in which higher temperature does not promote the crystallization of larger nanoparticles but increases their surface diffusion.

According to the EDX quantification, the elemental composition of the S-350 film is: C = 17.91 at. %, N = 21.13 at. %, Si = 18.77 at. % and Ti = 42.19 at. %. This elemental distribution clearly shows that the SiC layers have a composition close to the stoichiometric ratios.

SIMS analysis is shown in Fig. 6 and shows the entire structure of the S-350 film, with all the fifty eight bilayers sequentially separated. Sputtering with a 1.72 keV Ar^+ beam allows the removal of all the successive layers and registering ionic currents of characteristic secondary ions. Visible oscillations of the $^{48}Ti^+$, $^{28}Si^+$ and $^{12}C^+$ positive

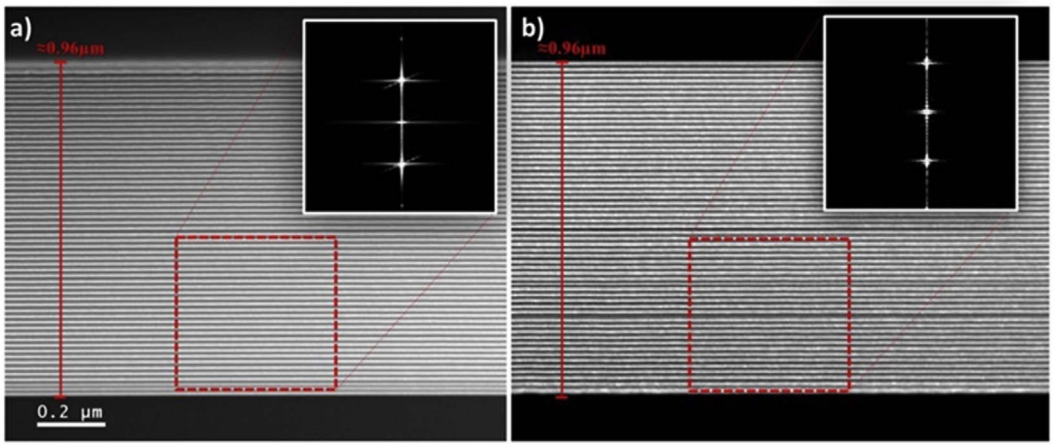

Fig. 4. Dark field image of the total thickness (~960 nm) of the 350 °C film (a). Similar image for the sample grown at 200 °C (b). The inset shows a self-correlation analysis for the estimate of the modulation period, with 200 °C ≈ 17 nm and 350 °C ≈ 16 nm congruent with the XRR data.

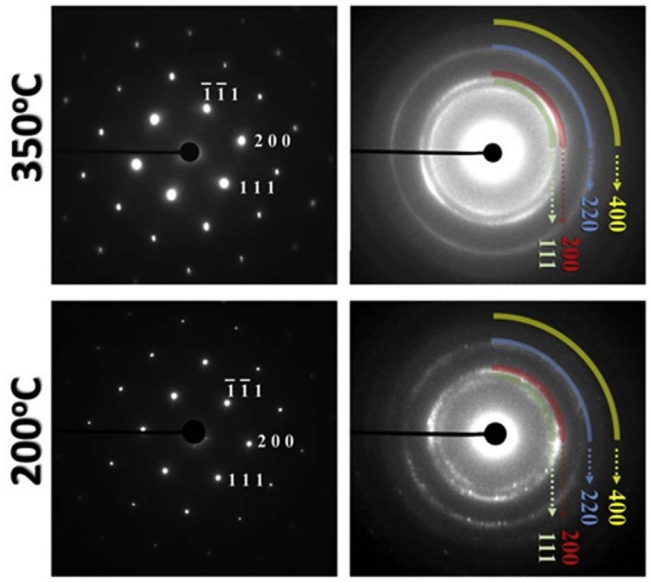

Fig. 5. Diffraction patterns collected over a 200 nm area of both the Si substrate (left) and the films (right), top 350 °C and bottom 200 °C.

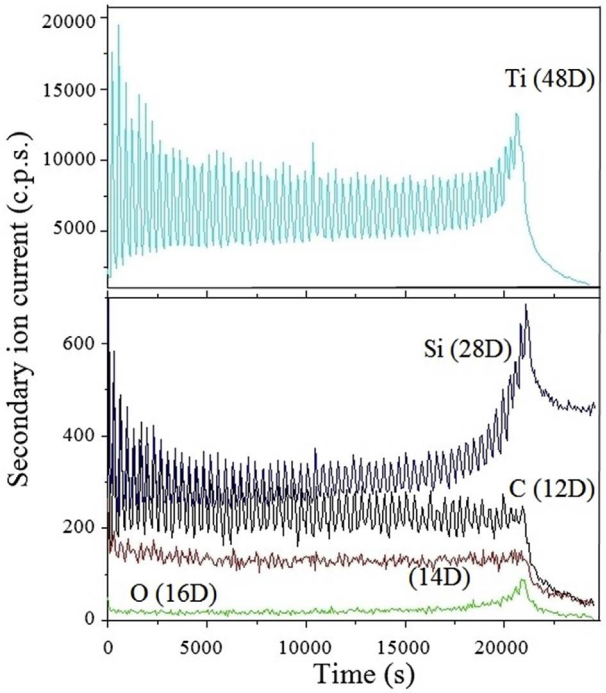

Fig. 6. SIMS depth profile analysis of the S-350 film. Registered are secondary ion currents of $^{12}C^+$ (12 D), $^{16}O^+$ (16 D), $^{28}Si^+$ (28 D) and $^{48}Ti^+$(48 D). The mass of 14 represents $^{12}CH_2{}^+$ and $^{28}Si^{++}$ ions rather than the $^{14}N^+$ ion current.

ion currents result from the ion etching of the successive layers of TiN and SiC. When the sputtering front approaches the Si substrate, the $^{48}Ti^+$ ion current gradually increases. This effect results from the increased oxygen concentration in the vicinity of the substrate. Residual oxygen contamination across the analysed structure is depicted by the $^{16}O^+$ ion current plot. Nitrogen detection in SIMS analysis is difficult, since the positive ion current of mass 14 D represents $^{12}CH_2{}^+$ and $^{28}Si^{++}$ ions rather than the $^{14}N^+$ ion current. In fact, the plot of mass 14 D does not show as clearly resolved oscillations as the plots of 12 D ($^{12}C^+$), 28 D ($^{28}Si^+$) and 48 D ($^{48}Ti^+$).

The XPS core level spectra and their fitting for the high temperature S-350 film are shown in Fig. 7. We performed the fitting of all the XPS spectra by GAUSSIAN software. The Ti 2p spectrum shows two main peaks. It is established that the Gaussian peak at 455.2 eV can be assigned to Ti $2p_{3/2}$ in TiN (455.1 eV [74], 455.2); the peak at 456.5 eV can be associated with TiNO (456.8 eV [74]); the peak at 458.3 eV is assigned to TiO_2 (458.3 eV [74]); the Gaussian peak at 461.0 eV corresponds to Ti $2p_{1/2}$ in TiN (460.6 eV [74], 460.9); the peak at 462.7 eV can be assigned to TiNO (462.5 eV [74]) and the peak at 464.7 eV – TiO_2 (464.0 eV [74], 464.7 eV). The N 1s spectrum is presented by two Gaussian curves with the peaks at 397.0 eV and 398.6 eV which can be assigned to TiN (397.0 eV) and to N – sp^3C (398.6 eV [75]), respectively. The Si 2p spectrum from the S-350 film exhibits one peak at 101.7 eV that can be assigned to Si-C bonds (101.8 eV [76]). The C 1s spectrum exhibits three features: the peak at 286.1 eV assigned to C bonded to N (C-N bonds, 286.1 eV [77]), the peak at 284.7 eV assigned to C bonded to C (C-C bonds, 284.6 eV [75]) and the peak at 282.5 eV assigned to C bonded to Si (Si-C bonds, 282.5 eV [76]). The fitted O 1s spectrum acquired from the S-350 film shows two peaks at 530.4 eV and 531.4 eV which are assigned to TiO_2 (530.4) and TiNO (531.3 eV), respectively.

From the analysis of the XRD (cf. Fig. 2) and XPS (cf. Fig. 7) spectra it follows that the main bonds in the film are Ti-N and Si-C, which are related to the TiN and SiC crystallites. Other bonds, such as Ti-N-O, Ti-O, C-N and C-C, are supposed to form by the atoms located at the interfaces. Results of XPS studies of the coating, which was deposited under the temperature 350 °C, showed that C-N 286.1 bond was

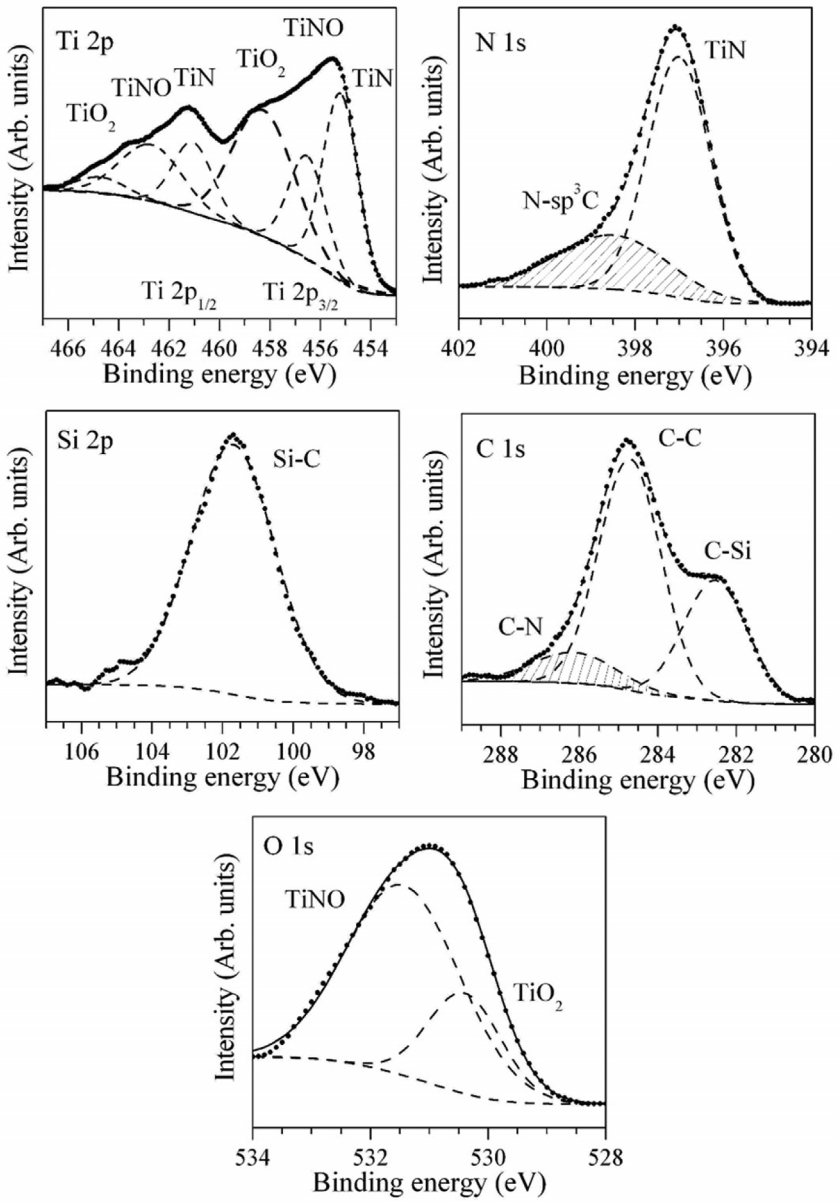

Fig. 7. XPS core level spectra for the S-350 film.

formed, and N bond with sp^3 C (398.6 eV) was formed in the TiN layers (397.0 eV). Thus, high deposition temperature led to interaction of some C atoms with crystal TiN phase, in its turn it led to forming of C-N bonds. This correlates with the results from SIMS studies, where some peaks from C are overlapping the TiN layers, especially when compared with the coatings, deposited at lower temperature T = 200 °C. Thus, we can make a conclusion that diffusion of C atoms into TiN layers takes place, and we can also make a prediction about diffusion of N atoms into SiC layers. In other words, both SIMS and XPS results indirectly confirms the forming of N-C bonds, while value content of these state can reach 12–15%.

We should point, that XPS is a direct method of defining of chemical bonds between amorphous SiC and nanocrystalline TiN on the interlayer boundary, whereas SIMS is an indirect one, allowing to study chemical bonds using changes in distribution of energy of secondary ions during sputtering. Displacement of some parts of Carbon profiles closer to Titanium ones (is not shown in Fig. 7), due to possible thermodiffusion when the substrate was heated to 350 °C during deposition, is an additional confirmation of our assumption.

In Fig. 8, we show the nanohardness (H), Knoop hardness (HK) and elastic modulus (E) of the deposited films depending on substrate temperature. One can see that the drastic increase in the values of H, HK and E occurs at $T_S > 100$ °C. We suppose that this is caused by the formation of crystallites in both the TiN and SiC layers in the high temperature films (cf. Figs. 2, 4 and 5). Knoop hardness was equal to 53 GPa and nanohardness reached the values of 32–34 GPa in the case of dynamic indentation mode, which is much higher, than in the works [56,57], in which nanohardness reaches the values around 18 GPa in the case of optimal thickness of the SiC layers (0.6 nm) and dynamic indentation mode. According to modern trends of forming of superhard (H ≥ 40 GPa) nanocomposite coatings [78], if the grains of one of the phases with the size around 10 nm are surrounded by an amorphous material from the other phase, the hardness of such coatings will achieve the values of 70–100 GPa. Our results clearly correlate with this theory, although our nanocrystalline phase has much smaller size.

It is clear at this point that the mixture of nanocomposite layers improves on the mechanical response of the samples, however, the mechanical increment observed, does not follow well the typical example of multi-layered samples, in which crystalline interfaces dissipate shear stress and allocate strain. Therefore, it is sensible to assume, that

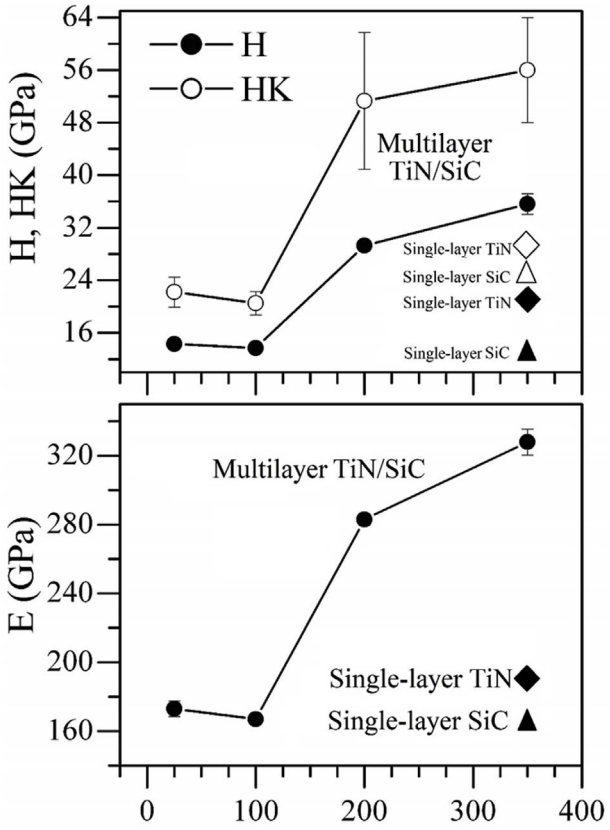

Fig. 8. Nanohardness (H), Knoop hardness (HK) and elastic modulus (E) for single-layer TiN and SiC films (◇△▲◆) and for TiN/SiC multilayers (●○) as a function of temperature.

interstitial effects and rearrangements, between the TiN/SiC phases are playing some role in the enhanced mechanical response. Our experiments have clearly pointed to a change in the modulation period of the samples, pointing to interfacial reactions, diffusion of ions or crystallization of new phases. Additionally, our SIMS and XPS data clearly point to interstitial reactions between TiN and SiC. Therefore it is sensible to assume that crystallites at the boundaries of TiN and SiC can be responsible for the hardness increment and the physico-chemical changes in the samples.

3.2. Theoretical results and the interpretation of experimental data

To understand the dependency of the mechanical performance on substrate temperature established above for multilayer TiN/SiC films, and to stablish the feasibility of interstitial crystallites, we investigated the TiN/SiC heterostructures generated at different temperatures (cf. Sec. 2). Due to the nanocomposite nature of the films and their inherent polycrystallinity, a simple, but representative, crystalline configuration had to be selected. Thus, the TiN(001) was selected, since those reflections were predominant in the XRD spectra of the deposited films (cf. Fig. 2), thus, our system is TiN(001)/SiC. In Fig. 9, the atomic configurations of the heterostructures under consideration are shown at different stages of elongation. In the low temperature B1-heterostructure, the epitaxial interfacial B1-SiC layer is preserved (the B1 heterostructure). However, this interfacial layer undergoes structural transformation at high temperature. An analysis of the atomic configuration and structural functions (not shown here) of this high temperature interface clearly shows that it consists of the 3C-SiC-like layers (the B3 heterostructure). The amorphous SiC interface (the A0 heterostructure) is weakly influenced by heating up to 300 K. The heating to 1200 K and slow cooling to 300 K transform this interface to the strongly distorted 3C-SiC layers (cf. Fig. 9, A1, $\varepsilon = 0.0$). It follows that both the B1- and a-SiC-interfaces transform into the 3C-SiC-like ones at high temperature.

We also investigated the behaviour of the heterostructures under tensile strain. The stress-tensile strain relations are shown in Fig. 10, and the atomic configurations just after failure are shown in Fig. 9. The ideal tensile strengths (σ_T, the maximum achieved stress under tensile strain) of the B1, B3, A0 and A1 heterostructures are 16 GPa, 17 GPa, 8 GPa and 11 GPa, respectively. Taking into account this finding, one can suppose that the three-layer 3C-SiC interface will be the most stable one among other interfaces considered here. The weakest interface is the A0 one (the a-SiC interface). So, the formation of the amorphous interfaces in the TiN(001)/SiC heterostructures will lead to reducing their mechanical performance. We note one interesting feature: all the interfaces in the TiN(001)/SiC heterostructures after failure undergo the same structural transformation. In this way, their structures become close to the strongly distorted 3C-SiC (cf. Fig. 9). However, there are the differences in the mechanisms of their failure. All the heterostructures (except for the B3 heterostructure) fail due to the delamination of the TiN and SiC layers. In the case of the B3 heterostructure, the interface is so strong that the failure occurs mainly in the TiN slab (cf. Fig. 9).

For the sake of comparison, the ideal tensile strength of the TiN (001)/one layer 3C-SiC heterostructure (~12 GPa) [58] is lower than that of the TiN(001)/three layer 3C-SiC heterostructure considered here. On the other hand, the value of σ_T of the TiN(001)/one layer B1-SiC heterostructure (24 GPa) [58] is much higher compared to the ideal tensile strength of the TiN(001)/three layer B1-SiC heterostructure. Based on these results, we can suppose that, for the TiN(001)/SiC heterostructure, the thinner the B1-SiC interfacial layer, the higher its strength. On the contrary, to reach the maximum strength, the B3-SiC interface should consist of more than one 3C-SiC layer.

The question to be addressed is the origin of the temperature-induced instability of the B1-SiC interface in the TiN(001)/SiC heterostructure. To answer this question, we investigated the behaviour of the $\Delta_{5'}$ phonon soft mode for B1-SiC as a function of the Si-C bond-length (R_{Si-C}). In Fig. 11, we show the frequency of the $\Delta_{5'}$ soft phonon mode as a function of R_{Si-C}. The negative (imaginary) frequencies are present in the phonon spectrum of B1-SiC for $R_{Si-C} > 2.136$ Å. The Ti-N bond-length in our heterostructures is 2.124 Å. It follows that the B1-SiC interface is quite stable and can form between the TiN layers at low temperatures. However, it becomes unstable with increasing temperature owing to lattice expansion when R_{Si-C} becomes larger than 2.136 Å (cf. Fig. 11).

Returning to our films, we will use these theoretical findings to interpret film properties. As mentioned above, the low temperature films have amorphous SiC layers and possess low hardness. It was supposed that the formation of SiC crystallites in the SiC layers would lead to improving the mechanical properties of the high temperature films. This supposition is quite consistent with our theoretical results: an increase in growth temperature leads to the formation of the 3C-SiC-like interfaces in the TiN(001)/SiC heterostructures that are responsible for their strengthening. On the other hand, the multilayer TiN/SiC films with nanocrystalline TiN layers and very thin SiC layers (the thickness was ~0.6 nm), deposited under other conditions and at room temperature, exhibit a superior hardness above 60 GPa [56,57]. According to our calculations, in such structures will form the B1-SiC-like layers. The ideal tensile strength of the TiN(001)/one layer B1-SiC heterostructure is comparable with that of the TiN(001)/three layer 3C-SiC one (cf. Fig. 8 in Ref. [58] and Fig. 10 in the present investigation). So, there are two ways to increase the strength of the TiN/SiC nanolayered films: 1) the films should be deposited at low temperatures to provide the formation of thin highly oriented B1-SiC layers; 2) the films should be deposited at moderate substrate temperatures to guarantee the formation of the heteroepitaxial cubic or hexagonal SiC interfaces that contain more than one SiC monolayer.

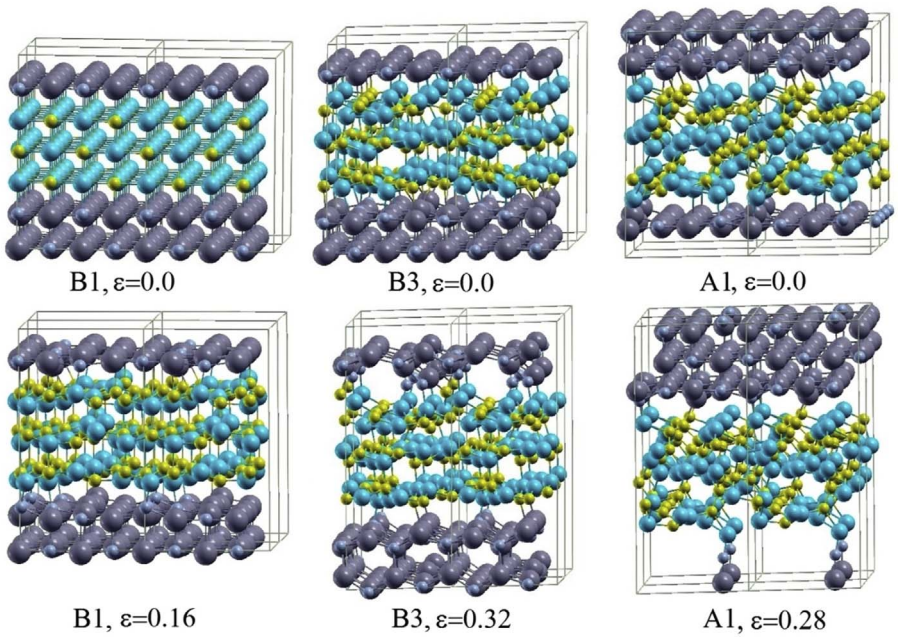

Fig. 9. Atomic configurations of the TiN(001)/SiC heterostructures at different stages of elongation. The notation of the samples is described in Sec. 2.

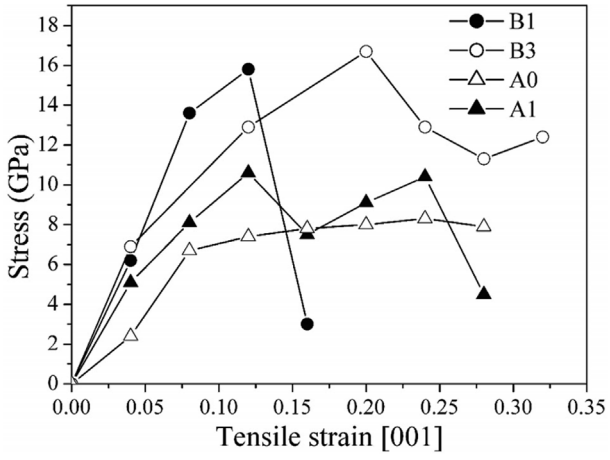

Fig. 10. Stress-tensile strain curves for the TiN(001)/SiC heterostructures generated under different conditions.

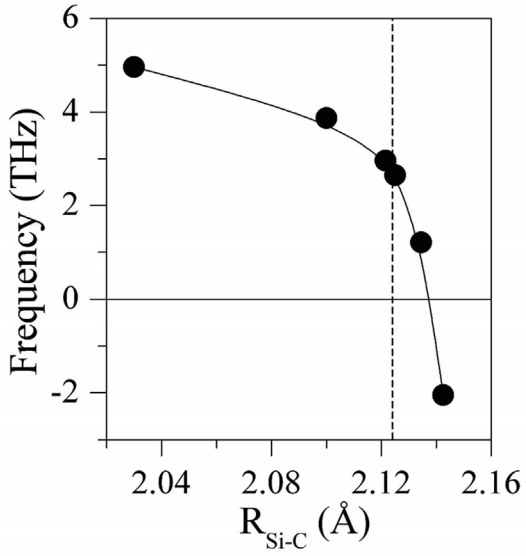

Fig. 11. Frequency of the soft phonon mode $\Delta_{5'}$ [2π/a(1/4,0,0)] as a function of the length of the Si-C bonds (R_{Si-C}) for B1-SiC. The solid line is a polynomial fitting to the calculated points. The vertical dotted line denotes R_{Si-C} in TiN.

4. Conclusions

Nanoscale multilayer TiN/SiC films were deposited at various substrate temperatures using sequential magnetron sputtering of TiN and SiC targets. The deposited films were studied by using XRD, XPS, FTIR, TEM, SIMS techniques, as well as nano- and micro-indentation analysis. First-principles molecular dynamics simulations of the TiN/SiC heterostructures were carried out to provide more precise analysis of the multilayer films properties. The films deposited at low substrate temperatures (up to 100 °C) represent the sequence of the nanocrystalline TiN layers and the amorphous SiC (a-SiC) layers. A further increase in substrate temperature led to the formation of the crystallites in both the TiN and SiC layers. Therefore, the nanohardness, Knoop hardness and elastic modulus increased abruptly to 32–34 GPa to 56 GPa and 330 GPa, respectively. It was found that the high temperature films have distinct interfaces. The main bonds in the high temperature films are Ti-N and Si-C originating from the TiN and SiC crystallites. Other bonds, such as Ti-N-O, Ti-O, C-N and C-C, are supposed to be formed by the atoms located at the interfaces. It is expected that C-N, (Ti,Si)C-N and Ti-Si-(N,C) interfacial reactions take place due to the rich interface energy, specially evidence by the remanence of the nanocomposite structure of the coatings, scenario that could address the improvement of mechanical response.

The calculations of the TiN(001)/SiC heterostructures generated at various conditions showed that the B1-SiC interface is quite stable and can be formed between TiN layers at low temperatures. However, it becomes unstable with increasing temperature due to lattice expansion. Based on the theoretical results, we suppose that, for the TiN(001)/SiC heterostructure, the thinner the B1-SiC interfacial layer, the higher its strength. On the contrary, to reach the maximum strength, the B3-SiC interface should consist of more than one SiC layer.

Using the experimental and theoretical results of the present work and those gained in other investigations, we come to the conclusion that there are two ways to increase the strength of the TiN/SiC nanolayered films: 1) the films are to be deposited at low temperatures to provide the formation of thin epitaxial B1-SiC layers (for < 3 nm thick films); 2) for thicker SiC layers (> 3 nm) the films are to be deposited at

moderate substrate temperatures to guarantee the formation of the heteroepitaxial cubic or hexagonal SiC interfaces that contain more than one SiC monolayer.

The results presented in this paper provide useful guidance to researchers who are interested in the synthesis of nanolayered thin films based on transition metal nitrides. Nevertheless, further studies are needed in order to investigate the nanocrystalline evolution of the interstitial crystals and their influence on the overall mechanical behaviour of nanocomposite layers, especially the apparition and role of (Ti,Si)C-N and Ti-Si-(N,C) interfacial phases.

Author contributions

Alexander Pogrebnjak: Project conception, Analysis of results and General supervision, **Volodymyr Ivashchenko and Petro Skrynskyy**: Simulations and XPS experiments, **Oleksandr Bondar**: Growth of laminates, Analysis of Results and Manuscript preparation; **Piotr Konarski**: SiMS Experiments; **Karol Zaleski**: FIB cross sections; **Stefan Jurga**: Project supervision and **Emerson Coy**: XRD, XRR, HR-TEM, Nanoindentation, Analysis of Results and Manuscript Preparation.

Acknowledgements

This work was supported by the Contract III-9-15 of NAS of Ukraine and was performed under the aegis of Ukrainian state budget programs: “Development of material science fundamentals of structure engineering of vacuum-plasma superhard coatings with given functional properties” (registration number 0115U000682) and “Development of perspective nanostructured multilayered coatings with enhanced physical-mechanical and tribological properties” (registration number 0116U006816). We are grateful to Dr.Sci. M.V. Karpets and Dr. I.I. Timofeeva for XRD measurements, Dr.Sci. S.N. Dub for nanoindentation tests and Dr O.K. Sinelnichenko for XPS measurements.

References

[1] Xu L, Li S, Zhang Y, Zhai Y. Synthesis, properties and applications of nanoscale nitrides, borides and carbides. Nanoscale 2012;4:4900. http://dx.doi.org/10.1039/c2nr30598d.

[2] Ferrari AC, Bonaccorso F, Fal'ko V, Novoselov KS, Roche S, Bøggild P, et al. Science and technology roadmap for graphene, related two-dimensional crystals, and hybrid systems. Nanoscale 2015;7:4598–810. http://dx.doi.org/10.1039/C4NR01600A.

[3] Thomson D, Zilkie A, Bowers JE, Komljenovic T, Reed GT, Vivien L, et al. Roadmap on silicon photonics. J Opt 2016;18:73003http://dx.doi.org/10.1088/2040-8978/18/7/073003.

[4] Li X, Liu X. Group III nitride nanomaterials for biosensing. Nanoscale 2017;9:7320–41. http://dx.doi.org/10.1039/C7NR01577A.

[5] Kindlund H, Sangiovanni DG, Martínez-de-Olcoz L, Lu J, Jensen J, Birch J, et al. Toughness enhancement in hard ceramic thin films by alloy design. APL Mater 2013;1:42104http://dx.doi.org/10.1063/1.4822440.

[6] Sangiovanni DG, Hultman L, Chirita V, Petrov I, Greene JE. Effects of phase stability, lattice ordering, and electron density on plastic deformation in cubic TiWN pseudobinary transition-metal nitride alloys. Acta Mater 2016;103:823–35. http://dx.doi.org/10.1016/j.actamat.2015.10.039.

[7] Joelsson T, Hultman L, Hugosson HW, Molina-Aldareguia JM. Phase stability tuning in the NbxZr1 − xN thin-film system for large stacking fault density and enhanced mechanical strength. Appl Phys Lett 2005;86:131922http://dx.doi.org/10.1063/1.1884743.

[8] Hugosson HW, Jansson U, Johansson B, Eriksson O. Restricting dislocation movement in transition metal carbides by phase stability tuning. Science (80) 2001;293:2434–7. http://dx.doi.org/10.1126/science.1060512.

[9] Kindlund H, Sangiovanni DG, Lu J, Jensen J, Chirita V, Birch J, et al. Vacancy-induced toughening in hard single-crystal V0.5Mo0.5Nx/MgO(001) thin films. Acta Mater 2014;77:394–400. http://dx.doi.org/10.1016/j.actamat.2014.06.025.

[10] Sangiovanni DG, Chirita V, Hultman L. Electronic mechanism for toughness enhancement in TixM1 − xN(M = Mo and W). Phys Rev B 2010;81:104107http://dx.doi.org/10.1103/PhysRevB.81.104107.

[11] Jhi S-H, Ihm J, Louie SG, Cohen ML. Electronic mechanism of hardness enhancement in transition-metal carbonitrides. Nature 1999;399:132–4. http://dx.doi.org/10.1038/20148.

[12] Sangiovanni DG, Hultman L, Chirita V. Supertoughening in B1 transition metal nitride alloys by increased valence electron concentration. Acta Mater 2011;59:2121–34. http://dx.doi.org/10.1016/j.actamat.2010.12.013.

[13] Sangiovanni DG, Hultman L, Chirita V, Petrov I, Greene JE. Effects of phase stability, lattice ordering, and electron density on plastic deformation in cubic TiWN pseudobinary transition-metal nitride alloys. Acta Mater 2016;103:823–35. http://dx.doi.org/10.1016/j.actamat.2015.10.039.

[14] Steneteg P, Hellman O, Vekilova OY, Shulumba N, Tasnádi F, Abrikosov IA. Temperature dependence of TiN elastic constants from ab initio molecular dynamics simulations. Phys Rev B 2013;87:94114http://dx.doi.org/10.1103/PhysRevB.87.094114.

[15] Rachbauer R, Massl S, Stergar E, Holec D, Kiener D, Keckes J, et al. Decomposition pathways in age hardening of Ti-Al-N films. J Appl Phys 2011;110:23515http://dx.doi.org/10.1063/1.3610451.

[16] Mikula M, Plašienka D, Sangiovanni DG, Sahul M, Roch T, Truchlý M, et al. Toughness enhancement in highly NbN-alloyed Ti-Al-N hard coatings. Acta Mater 2016;121:59–67. http://dx.doi.org/10.1016/j.actamat.2016.08.084.

[17] Lind H, Forsén R, Alling B, Ghafoor N, Tasnádi F, Johansson MP, et al. Improving thermal stability of hard coating films via a concept of multicomponent alloying. Appl Phys Lett 2011;99:91903http://dx.doi.org/10.1063/1.3631672.

[18] Mikula M, Plašienka D, Roch T, Štyráková K, Satrapinskyy L, Drienovský M, et al. Structural evolution of TaN-alloyed Cr–Al–Y–N coatings. Surf Coating Technol 2016;288:203–10. http://dx.doi.org/10.1016/j.surfcoat.2016.01.031.

[19] Mikula M, Sangiovanni DG, Plašienka D, Roch T, Čaplovičová M, Truchlý M, et al. Thermally induced age hardening in tough Ta-Al-N coatings via spinodal decomposition. J Appl Phys 2017;121:155304http://dx.doi.org/10.1063/1.4981534.

[20] Pogrebnjak AD, Yakushchenko IV, Bondar OV, Beresnev VM, Oyoshi K, Ivasishin OM, et al. Irradiation resistance, microstructure and mechanical properties of nanostructured (TiZrHfVNbTa)N coatings. J Alloys Compd 2016;679:155–63. http://dx.doi.org/10.1016/j.jallcom.2016.04.064.

[21] Pogrebnjak AD, Bagdasaryan AA, Yakushchenko IV, Beresnev VM. The structure and properties of high-entropy alloys and nitride coatings based on them. Russ Chem Rev 2014;83:1027–61. http://dx.doi.org/10.1070/RCR4407.

[22] Pogrebnjak AD, Yakushchenko IV, Bondar OV, Sobol' OV, Beresnev VM, Oyoshi K, et al. Influence of implantation of Au − ions on the microstructure and mechanical properties of the nanostructured multielement (TiZrHf VNbTa)N coating. Phys Solid State 2015;57:1559–64. http://dx.doi.org/10.1134/S1063783415080259.

[23] Svito I, Fedotova JA, Milosavljević M, Zhukowski P, Koltunowicz TN, Saad A, et al. Influence of sputtering atmosphere on hopping conductance in granular nanocomposite (FeCoZr)x(Al2O3)1 − x films. J Alloys Compd 2014;615:S344–7. http://dx.doi.org/10.1016/j.jallcom.2013.12.061.

[24] Yate L, Emerson Coy L, Wang G, Beltrán M, Díaz-Barriga E, Saucedo EM, et al. Tailoring mechanical properties and electrical conductivity of flexible niobium carbide nanocomposite thin films. RSC Adv 2014;4:61355–62. http://dx.doi.org/10.1039/C4RA11292J.

[25] Pogrebnjak A, Rogoz V, Ivashchenko V, Bondar O, Shevchenko V, Jurga S, et al. Nanocomposite Nb-Al-N coatings: experimental and theoretical principles of phase transformations. J Alloys Compd 2017;718:260–9. http://dx.doi.org/10.1016/j.jallcom.2017.05.136.

[26] Chen CQ, Pei YT, Shaha KP, De Hosson JTM. Nanoscale deformation mechanism of TiC/a-C nanocomposite thin films. J Appl Phys 2009;105:114314http://dx.doi.org/10.1063/1.3130123.

[27] Pshyk AV, Coy LE, Yate L, Załęski K, Nowaczyk G, Pogrebnjak AD, et al. Combined reactive/non-reactive DC magnetron sputtering of high temperature composite AlN–TiB2–TiSi2. Mater Des 2016;94:230–9. http://dx.doi.org/10.1016/j.matdes.2015.12.174.

[28] Yate L, Coy LE, Gregurec D, Aperador W, Moya SE, Wang G. Nb–C nanocomposite films with enhanced biocompatibility and mechanical properties for hard-tissue implant applications. ACS Appl Mater Interfaces 2015;7:6351–8. http://dx.doi.org/10.1021/acsami.5b01193.

[29] Coy E, Yate L, Valencia DP, Aperador W, Siuzdak K, Torruella P, et al. High electrocatalytic response of a mechanically enhanced NbC nanocomposite electrode toward hydrogen evolution reaction. ACS Appl Mater Interfaces 2017;9:30872–9. http://dx.doi.org/10.1021/acsami.7b10317.

[30] Weber M, Coy E, Iatsunskyi I, Yate L, Miele P, Bechelany M. Mechanical properties of boron nitride thin films prepared by atomic layer deposition. CrystEngComm 2017;19:6089–94. http://dx.doi.org/10.1039/C7CE01357D.

[31] Hugosson HW. Restricting dislocation movement in transition metal carbides by phase stability tuning. Science (80) 2001;293:2434–7. http://dx.doi.org/10.1126/science.1060512.

[32] Hu C, Huang J, Sumpter BG, Meletis E, Dumitrică T. Ab initio predictions of hexagonal Zr(B, C,N) polymorphs for coherent interface design. J Phys Chem C 2017;121:26007–18. http://dx.doi.org/10.1021/acs.jpcc.7b09444.

[33] Music D, Geyer RW, Schneider JM. Recent progress and new directions in density functional theory based design of hard coatings. Surf Coating Technol 2016;286:178–90. http://dx.doi.org/10.1016/j.surfcoat.2015.12.021.

[34] Liu ZTY, Gall D, Khare SV. Electronic and bonding analysis of hardness in pyrite-type transition-metal pernitrides. Phys Rev B 2014;90:134102http://dx.doi.org/10.1103/PhysRevB.90.134102.

[35] Dehgahi S, Amini R, Alizadeh M. Corrosion, passivation and wear behaviors of electrodeposited Ni–Al2O3–SiC nano-composite coatings. Surf Coating Technol 2016;304:502–11. http://dx.doi.org/10.1016/j.surfcoat.2016.07.007.

[36] Hu M, Li K, Li H, Feng T, Li L. Influence of β-SiC on the microstructures and thermal properties of SiC coatings for C/C composites. Surf Coating Technol 2016;304:188–94. http://dx.doi.org/10.1016/j.surfcoat.2016.07.010.

[37] Pourasad J, Ehsani N. In-situ synthesis of SiC-ZrB2 coating by a novel pack cementation technique to protect graphite against oxidation. J Alloys Compd 2017;690:692–8. http://dx.doi.org/10.1016/j.jallcom.2016.08.112.

[38] Wasekar NP, Latha SM, Ramakrishna M, Rao DS, Sundararajan G. Pulsed electrodeposition and mechanical properties of Ni-W/SiC nano-composite coatings. Mater Des 2016;112:140–50. http://dx.doi.org/10.1016/j.matdes.2016.09.070.

[39] Shypylenko A, Pshyk AV, Grześkowiak B, Medjanik K, Peplinska B, Oyoshi K, et al. Effect of ion implantation on the physical and mechanical properties of Ti-Si-N multifunctional coatings for biomedical applications. Mater Des 2016;110:821–9. http://dx.doi.org/10.1016/j.matdes.2016.08.050.
[40] Kabel J, Yang Y, Balooch M, Howard C, Koyanagi T, Terrani KA, et al. Micro-mechanical evaluation of SiC-SiC composite interphase properties and debond mechanisms. Compos Part B Eng 2017;131:173–83. http://dx.doi.org/10.1016/j.compositesb.2017.07.035.
[41] Ming J, Li M, Kumar P, Li L-J. Multilayer approach for advanced hybrid lithium battery. ACS Nano 2016;10:6037–44. http://dx.doi.org/10.1021/acsnano.6b01626.
[42] Madar R. Materials science: silicon carbide in contention. Nature 2004;430:974–5. http://dx.doi.org/10.1038/430974a.
[43] Wedig A, Luebben M, Cho D-Y, Moors M, Skaja K, Rana V, et al. Nanoscale cation motion in TaOx, HfOx and TiOx memristive systems. Nat Nanotechnol 2015;11:67–74. http://dx.doi.org/10.1038/nnano.2015.221.
[44] Chen ABK, Kim SG, Wang Y, Tung W-S, Chen I-W. A size-dependent nanoscale metal–insulator transition in random materials. Nat Nanotechnol 2011;6:237–41. http://dx.doi.org/10.1038/nnano.2011.21.
[45] López-Vidrier J, Löper P, Schnabel M, Hernández S, Canino M, Summonte C, et al. Silicon nanocrystals embedded in silicon carbide as a wide-band gap photovoltaic material. Sol Energy Mater Sol Cells 2016;144:551–8. http://dx.doi.org/10.1016/j.solmat.2015.10.006.
[46] Jia Y, Wang Y, Dong L, Huang J, Zhang Y, Su J, et al. A hybrid of titanium nitride and nitrogen-doped amorphous carbon supported on SiC as a noble metal-free electrocatalyst for oxygen reduction reaction. Chem Commun 2015;51:2625–8. http://dx.doi.org/10.1039/C4CC08007F.
[47] Juan JS, Nó ML, Schuh CA. Nanoscale shape-memory alloys for ultrahigh mechanical damping. Nat Nanotechnol 2009;4:415–9. http://dx.doi.org/10.1038/nnano.2009.142.
[48] So¨derberg H, Odén M, Molina-Aldareguia JM, Hultman L. Nanostructure formation during deposition of TiN/SiN[sub x] nanomultilayer films by reactive dual magnetron sputtering. J Appl Phys 2005;97:114327http://dx.doi.org/10.1063/1.1935135.
[49] So¨derberg H, Odén M, Larsson T, Hultman L, Molina-Aldareguia JM. Epitaxial stabilization of cubic-SiN[sub x] in TiN/SiN[sub x] multilayers. Appl Phys Lett 2006;88:191902http://dx.doi.org/10.1063/1.2202145.
[50] Hultman L, Bareño J, Flink A, Söderberg H, Larsson K, Petrova V, et al. Interface structure in superhard TiN-SiN nanolaminates and nanocomposites: film growth experiments and ab initio calculations. Phys Rev B 2007;75:155437http://dx.doi.org/10.1103/PhysRevB.75.155437.
[51] Fallqvist A, Ghafoor N, Fager H, Hultman L, Persson POA. Self-organization during growth of ZrN/SiNx multilayers by epitaxial lateral overgrowth. J Appl Phys 2013;114:224302http://dx.doi.org/10.1063/1.4838495.
[52] Ghafoor N, Lind H, Tasnádi F, Abrikosov IA, Odén M. Anomalous epitaxial stability of (001) interfaces in ZrN/SiNx multilayers. APL Mater 2014;2:46106http://dx.doi.org/10.1063/1.4870876.
[53] Setoyama M, Nakayama A, Tanaka M, Kitagawa N, Nomura T. Formation of cubic-AlN in TiN/AlN superlattice. Surf Coating Technol 1996;86–87:225–30. http://dx.doi.org/10.1016/S0257-8972(96)03033-2.
[54] Ivashchenko V, Veprek S, Pogrebnjak A, Postolnyi B. First-principles quantum molecular dynamics study of Ti x Zr 1 − x N(111)/SiN y heterostructures and comparison with experimental results. Sci Technol Adv Mater 2014;15:25007http://dx.doi.org/10.1088/1468-6996/15/2/025007.
[55] Krishna H, Shirato N, Yadavali S, Sachan R, Strader J, Kalyanaraman R. Self-Organization of nanoscale multilayer liquid metal films: experiment and theory. ACS Nano 2011;5:470–6. http://dx.doi.org/10.1021/nn1022632.
[56] Lao J, Shao N, Mei F, Li G, Gu M. Mutual promotion effect of crystal growth in TiN/SiC nanomultilayers. Appl Phys Lett 2005;86:11902http://dx.doi.org/10.1063/1.1844045.
[57] Kong M, Dai J, Lao J, Li G. Crystallization of amorphous SiC and superhardness effect in TiN/SiC nanomultilayers. Appl Surf Sci 2007;253:4734–9. http://dx.doi.org/10.1016/j.apsusc.2006.10.050.
[58] Ivashchenko VI, Veprek S, Turchi PEA, Shevchenko VI. First-principles study of TiN/SiC/TiN interfaces in superhard nanocomposites. Phys Rev B 2012;86:14110http://dx.doi.org/10.1103/PhysRevB.86.014110.
[59] Matocha K. Challenges in SiC power MOSFET design. Solid State Electron 2008;52:1631–5. http://dx.doi.org/10.1016/j.sse.2008.06.034.
[60] Riccio M, Castellazzi A, De Falco G, Irace A. Experimental analysis of electro-thermal instability in SiC Power MOSFETs. Microelectron Reliab 2013;53:1739–44. http://dx.doi.org/10.1016/j.microrel.2013.07.014.
[61] Roccaforte F, Fiorenza P, Greco G, Vivona M, Lo Nigro R, Giannazzo F, et al. Recent advances on dielectrics technology for SiC and GaN power devices. Appl Surf Sci 2014;301:9–18. http://dx.doi.org/10.1016/j.apsusc.2014.01.063.
[62] Car R, Parrinello M. Unified approach for molecular dynamics and density-functional theory. Phys Rev Lett 1985;55:2471–4. http://dx.doi.org/10.1103/PhysRevLett.55.2471.
[63] Konarski P, Mierzejewska A. B4C/Mo/Si and Ta2O5/Ta nanostructures analysed by ultra-low energy argon ion beams. Appl Surf Sci 2003;203–204:354–8. http://dx.doi.org/10.1016/S0169-4332(02)00675-X.
[64] Basu S, Hay JL, Swindeman JE, Oliver WC. Continuous dynamic analysis: evolution of elastic properties with strain. MRS Commun 2014;4:25–9. http://dx.doi.org/10.1557/mrc.2013.49.
[65] Giannozzi P, Baroni S, Bonini N, Calandra M, Car R, Cavazzoni C, et al. QUANTUM ESPRESSO: a modular and open-source software project for quantum simulations of materials. J Phys Condens Matter 2009;21:395502http://dx.doi.org/10.1088/0953-8984/21/39/395502.
[66] Pogrebnjak AD, Bondar OV, Abadias G, Ivashchenko V, Sobol OV, Jurga S, et al. Structural and mechanical properties of NbN and Nb-Si-N films: experiment and molecular dynamics simulations. Ceram Int 2016;42:11743–56. http://dx.doi.org/10.1016/j.ceramint.2016.04.095.
[67] Perdew JP, Burke K, Ernzerhof M. Generalized gradient approximation made simple. Phys Rev Lett 1996;77:3865–8.
[68] Vanderbilt D. Soft self-consistent pseudopotentials in a generalized eigenvalue formalism. Phys Rev B 1990;41:7892–5. http://dx.doi.org/10.1103/PhysRevB.41.7892.
[69] Monkhorst HJ, Pack JD. Special points for Brillouin-zone integrations. Phys Rev B 1976;13:5188–92. http://dx.doi.org/10.1103/PhysRevB.13.5188.
[70] Billeter SR, Curioni A, Andreoni W. Efficient linear scaling geometry optimization and transition-state search for direct wavefunction optimization schemes in density functional theory using a plane-wave basis. Comput Mater Sci 2003;27:437–45. http://dx.doi.org/10.1016/S0927-0256(03)00043-0.
[71] Baroni S, de Gironcoli S, Dal Corso A, Giannozzi P. Phonons and related crystal properties from density-functional perturbation theory. Rev Mod Phys 2001;73:515–62. http://dx.doi.org/10.1103/RevModPhys.73.515.
[72] Du X-W, Fu Y, Sun J, Yao P, Cui L. Intensive light emission from SiCN films by reactive RF magnetron sputtering. Mater Chem Phys 2007;103:456–60. http://dx.doi.org/10.1016/j.matchemphys.2007.02.053.
[73] Lee SH, Nam J-W, Lim KH, Lee J-J. Nanoscale mutilayer TiN/BN films deposited by plasma enhanced chemical vapor deposition. Surf Coating Technol 2003;174:758–61. http://dx.doi.org/10.1016/S0257-8972(03)00571-1.
[74] Cheng Y, Zheng YF. Surface characterization and mechanical property of TiN/Ti-coated NiTi alloy by PIIID. Surf Coating Technol 2007;201:6869–73. http://dx.doi.org/10.1016/j.surfcoat.2006.09.055.
[75] Ma S, Xu B, Wu G, Wang Y, Ma F, Ma D, et al. Microstructure and mechanical properties of SiCN hard films deposited by an arc enhanced magnetic sputtering hybrid system. Surf Coating Technol 2008;202:5379–82. http://dx.doi.org/10.1016/j.surfcoat.2008.06.057.
[76] Rahman MM, Hasan SK. Ellipsometric, XPS and FTIR study on SiCN films deposited by hot-wire chemical vapor deposition method. Mater Sci Semicond Process 2016;42:373–7. http://dx.doi.org/10.1016/j.mssp.2015.11.006.
[77] Peng Y, Zhou J, Zhao B, Tan X, Zhang Z. Structural and optical properties of the SiCN thin films prepared by reactive magnetron sputtering. Appl Surf Sci 2011;257:4010–3. http://dx.doi.org/10.1016/j.apsusc.2010.11.166.
[78] Veprek S, Reiprich S, Vepřek S, Reiprich S. A concept for the design of novel superhard coatings. Thin Solid Films 1995;268:64–71. http://dx.doi.org/10.1016/0040-6090(95)06695-0.